Green Chemistry

Design of supported organocatalysts from a biomass-derived difuran compound and catalytic assessment for lactose hydrolysis

Journal:	*Green Chemistry*
Manuscript ID	GC-ART-11-2022-004243.R1
Article Type:	Paper
Date Submitted by the Author:	09-Dec-2022
Complete List of Authors:	Chang, Hochan; University of Wisconsin Madison, Chemical and Biological Engineering Stamoulis, Alexios; University of Wisconsin-Madison, Department of Chemistry Huber, George; University of Wisconsin-Madison, Chemical and Biological Engineering Dumesic, James; University of Wisconsin Madison, Chemical and Biological Engineering; Great Lakes Bioenergy Research Center

ARTICLE

Design of supported organocatalysts from a biomass-derived difuran compound and catalytic assessment for lactose hydrolysis

Received 00th January 20xx,
Accepted 00th January 20xx

DOI: 10.1039/x0xx00000x

Hochan Chang[a], Alexios G. Stamoulis[b], George W. Huber[a], and James A. Dumesic[a,c]*

The engineered structures and active sites of enzyme catalysts give rise to high catalytic activity and selectivity toward desired reactions. We have employed a biomass-derived difuran compound to append N-substituted maleimides with amino acid (glutamic acid) substitution by Diels-Alder reaction to mimic the chemical functional groups that comprise the active site channels in enzyme catalysts. The difunctionality of the biomass-derived difuran allows production of Diels-Alder adducts by appending two amino acid moieties to form a difunctional organocatalyst. The catalytic activity of the organocatalyst can be improved by immobilizing the organocatalyst on solid supporting materials. Accordingly, the structures of these immobilized organocatalysts can be engineered to mimic enzymatic active sites and to control the interaction between reactants, products, and transition states of catalytic reactions. Lactose hydrolysis was carried out to provide an example of industrial application of this approach to design and fabricate new supported organocatalysts as artificial enzymes.

1. Introduction

The cellulose fraction of lignocellulosic biomass is a sustainable carbon resource due to its natural abundance.[1,2] Catalytic conversion reactions of cellulose have been utilized to synthesize platform chemicals that are comprised of various oxygen-containing functional groups that are challenging to be synthesized from petroleum resources. [1] 5-hydroxymethyl furfural (HMF) has been produced as an important renewable platform chemical [3,4] because it possesses oxygen-containing functionalities, such as hydroxyl, aldehyde, and furan in its molecular structure. HMF has been used to synthesize diverse commodity chemicals, including liquid fuels [5] and monomers for production of polymers. [6] For example, HMF can be oxidized over metal catalysts and converted to 2,5-furan dicarboxylic acid (FDCA) [7] for the synthesis of polyethylene furanoate (PEF) as a replacement for polyethylene terephthalate (PET) [8]. Hydrodeoxygenation of HMF can produce 2,5-dimethylfuran (DMF) which can be used directly as a gasoline additive [5] or further upgraded to *p*-xylene after sequential Diels-Alder reaction and dehydration in the presence of zeolite catalysts. [9] Aldol condensation of HMF and ketones can also be used to synthesize new platform chemicals that have higher molecular weight. [10–12] Thus, biomass-derived HMF is one of important platform molecules to develop sustainable manufacture of value-added chemicals.

Diels-Alder reactions are powerful tools for not only petrochemical [13,14] but also biomedical applications [15] because these reactions can append additional functionalities onto molecules. In addition, reversible Diels-Alder linkages have served as a tool for click chemistry at elevated temperatures or in the presence of Brønsted acids. [16] An example of Diels-Alder reactions is the reaction of furan and maleimide moieties to synthesize valuable functionalities, such as norcantharimides [17] and phthalimides [18,19] that play critical roles in active pharmaceutical ingredients, like cantharidin and thalidomide derivatives. In our previous work, we have synthesized a HMF-derived platform chemical, denoted as HMF-Acetone-HMF (HAH), as a difuran resource by aldol-condensation of HMF and acetone. [20] The enone moiety in the HAH molecule acts an electron-withdrawing group and prevents the furan moiety in HAH from being an electron-rich furan, which is required for spontaneous Diels-Alder reaction with maleimide. Therefore, the furan moiety in HAH must be activated for Diels-Alder reaction by selective hydrogenation of the enone group. After the enone group in HAH has been selectively hydrogenated [21], the partially hydrogenated HAH (PHAH) can be used as a monomer for the synthesis of Diels-Alder adducts that can be used to design performance-advantaged plastics [22].

Enzymes are used in dairy [23–25] and biorefinery applications [26] because of their superior activity and selectivity for desired chemical reactions. The active site channels in enzymes are comprised of unique spatial and chemical structures to contribute to site-specific activities for target reactions. For instance, spatially-close amino acids residues, such as histidine, aspartate, and serine, form “catalytic triads” and play a role as active sites for chymotrypsin hydrolases. [27] Therefore, the control of physical space and the combination of chemical functionalities are of importance to develop enzyme or supported organocatalysts as artificial enzymes. Whereas the superior activity of enzymes is desirable for catalytic processes,

[a] *Department of Chemical and Biological Engineering, University of Wisconsin–Madison, Madison, WI, USA.*
[b] *Department of Chemistry, University of Wisconsin–Madison, Madison, WI, USA.*
[c] *DOE Great Lakes Bioenergy Research Center, University of Wisconsin–Madison, 1552 University Avenue, Madison, WI, USA.*
† Footnotes relating to the title and/or authors should appear here.
Electronic Supplementary Information (ESI) available: [details of any supplementary information available should be included here]. See DOI: 10.1039/x0xx00000x

the applications of enzymes can be limited by separation processes after reaction, and immobilization of enzymes can decrease the catalytic activity. [28] Moreover, enzymatic reactions require the use of biological media, containing nutrients in aqueous buffers, to achieve high activity and selectivity, and the use of the aqueous buffer media gives rise to severe separation and/or distillation steps for downstream processes. [29] These limitations of enzymatic reactions increase the production cost of the final products and can limit the selection of reaction conditions in downstream processes. Accordingly, development of chemical catalysts from sustainable resources that can function through enzymatic mechanisms and are analogous to enzymatic processes [30] is of critical importance for sustainable and economical processes. Previous research on the synthesis of artificial enzymes has been restricted due to the limited degrees of freedom to engineer the active sites on solid supports. For example, the catalytic activities of silica and alumina for polyglucans hydrolysis were limited by the maximum density of Brønsted acidic -OH sites. [31] Furthermore, the catalytic active sites were limited to molecules with simple structures when the chemicals were added to solid supports by grafting methods. [32]

In this paper, we show how we can design new classes of organocatalysts by carefully engineering the active sites using biomass-derived molecules. We have synthesized organocatalysts, including a difunctional organocatalyst from biomass-derived difuran, and we have demonstrated the catalytic properties of the organocatalysts for lactose hydrolysis as a model reaction. These organocatalysts were engineered by imidation, Diels-Alder reaction, and hydrogenation. The organocatalyst complexes were then deposited onto various solid supports, consisting of commercially produced materials (e.g., functionalize silicas, silicon carbide, TiO_2) to resemble protein frameworks in enzyme catalysts. The synthetic pathways for the immobilized organocatalysts displayed in Scheme 1a. The catalytic activities of these immobilized materials for lactose hydrolysis were 5.2 times higher (Figure 8) than glutamic acid, which is a chemical functionality in the active sites of lactase. The difunctionality of the organocatalyst and/or the control of the catalyst loading can be used in the future to further enhance the catalytic activity. The total carbon balance of the reaction system was higher than 95 mol% during lactose hydrolysis at 77 mol% conversion of lactose in the presence of the organocatalyst. The loss of 5 mol% carbon resulted from the degradation of glucose that produces reactive furan-containing by-products, like humins (Scheme 1b). The minor carbon loss (<5 mol%) throughout the reaction indicates the high catalytic selectivity of the organocatalysts. These results show that the design of the active sites in the molecules and the catalyst immobilization can provide new types of supported organocatalysts, which could have superior catalytic activity and selectivity for hydrolysis. Furthermore, the comparison of reaction kinetics for hydrolysis using various organocatalysts indicates that the catalytic activities of the organocatalysts can be modified by engineering the active sites, supports, and immobilization.

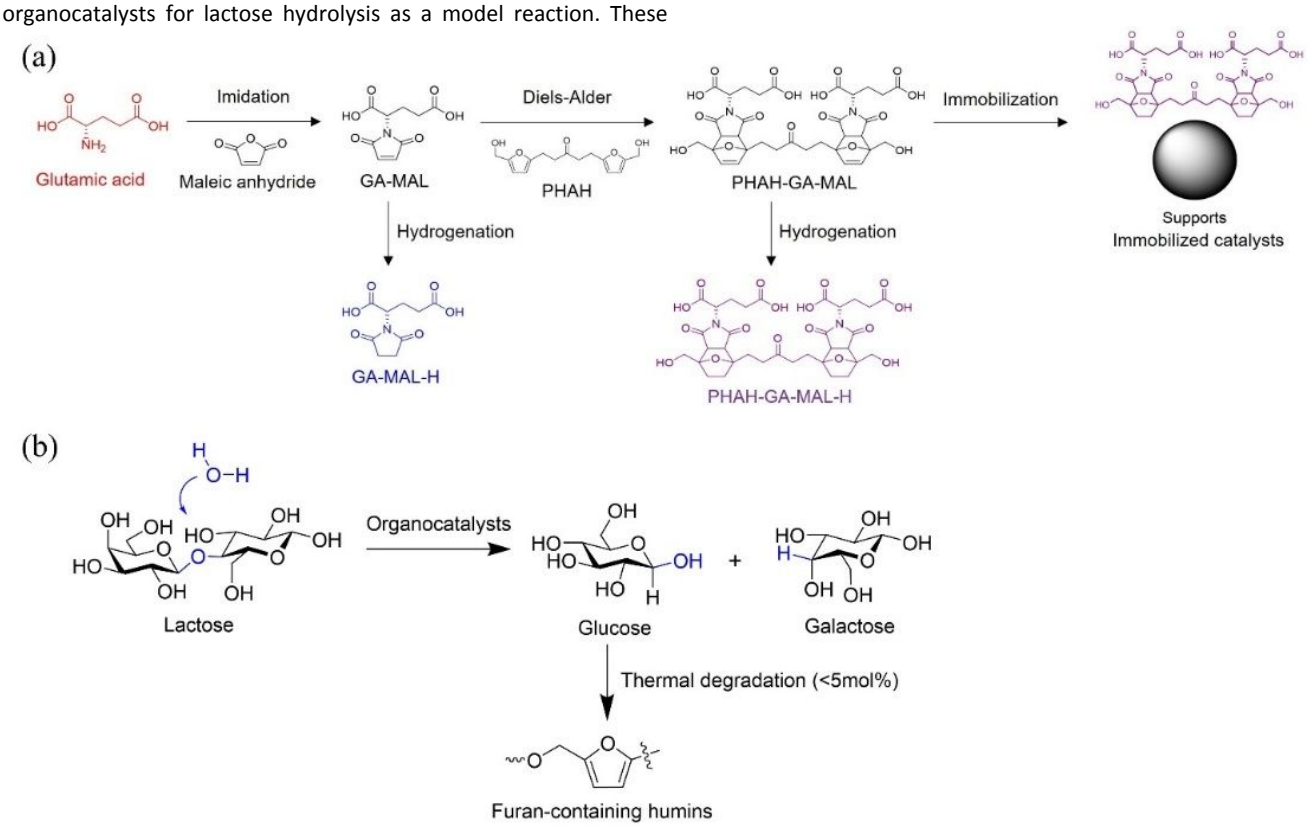

Scheme 1. (a) Reaction pathways for the synthesis of organocatalysts and immobilization of PHAH-GA-MAL-H on various supports (colored molecules represent organocatalysts), and (b) reaction routes for lactose hydrolysis in the presence of organocatalysts; Reaction conditions: 430 mM of lactose in water at 100°C, Organocatalysts: 16 wt% loading of organocatalyst on various supports (e.g., functionalized silicas, chemical-coated silicas, silicon carbide, TiO_2).

2. Experimental methods

2.1 Materials.

5-hydroxymethy furfural (HMF, AK Scientific, 98%), tetrahydrofuran (THF, Sigma-Aldrich, 250 ppm BHT as inhibitor, ACS reagent ≥99.0%), acetone (Fisher chemical, HPLC degree), NaOH (Honeywell, Reagent grade, pellets (anhydrous), ≥98%), HCl (Sigma-Aldrich, 37%), Mill-Q water (MQ water, ~18 MΩ cm), L-glutamic acid (Sigma-Aldrich, ReagentPlus, ≥99%), maleic anhydride (Fluka, puriss.: >99.0%), acetic acid (Sigma-Aldrich, ReagentPlus, ≥99%), sulfuric acid solution (Fluka, Reag. Ph. Eur., volumetric, 0.5M), L-alanine (Sigma-Aldrich, BioReagent), L-tyrosine (Sigma-Aldrich, BioUltra, ≥99.0%), taurine (Fluka, puriss. p,a,: >99.0%), calcium acetate hydrate ($Ca(OAc)_2$, Sigma-Aldrich, BioUltra, ≥99.0%), D-lactose monohydrate (Sigma-Aldrich, BioUltra, ≥99.5%), D-galactose (Sigma-Aldrich, ≥99%), D-glucose (Sigma-Aldrich, ≥99.5%), silica gel (Sigma-Aldrich, Davisil grade 646), mesoporous SBA-15 (Sigma-Aldrich, <150μm particle size, 4 and 6 nm pore size), silicon carbide (Sigma-Aldrich, 250-450 mesh particle size), Si-diol (SiliCycle, SiliaBond Diol nec, R35030B), Si-C_1 (SiliCycle, SiliaBond C1, R33030B), Si-C_4 (SiliCycle, SiliaBond C4, R32030B), Si-C_{18} (SiliCycle, SiliaBond C18, R33230B), TiO_2 (TiO_2-P25, Acros Organics), sucrose (Sigma-Aldrich, BioXtra, ≥99.5%), acetamide (Sigma-Aldrich, ≥99.0%), Cu/Al_2O_3 (Riogen, >98%, 5 wt% Cu loading), 2-propanol (IPA, Fisher chemical, HPLC degree). The above chemicals and materials were used without further purification.

2.2 Synthesis of PHAH by aldol-condensation and hydrogenation [21].

The aldol-condensed chemical consisting of two HMF (5-hydroxymenthyl furfural) and acetone is denoted as HAH. 1.83 g of NaOH was dissolved in 15 g of Milli-Q water to prepare 3 M of NaOH solution to catalyze aldol-condensation, and 2 mL of 37% HCl and 10 g of Milli-Q water were mixed to prepare 2 M of HCl solution to neutralize the NaOH catalyst after aldol-condensation. 10.2 g of HMF, 3 mL of acetone, and 71.28 mL of Milli-Q water were mixed in a 500 mL round bottom flask with magnetic stirring bar and placed in an oil bath at 35℃ for 5 min. 6.67 mL of 3 M of NaOH solution was added to the HMF and acetone solution, and the flask was capped with a glass lid. After 1 h of aldol-condensation, ~7.74 mL of 2 M of HCl solution was added to the flask to terminate aldol-condensation by neutralization. A pH strip was used to measure the pH of the aldol-condensed solution. The aldol-condensed solution with the precipitated HAH was vacuum filtered by paper while rinsing with ~300 mL of Milli-Q water. The washed HAH was dried in a vacuum oven at 50℃, under 500-600 mbar for 2 days.

Partially hydrogenated HAH is denoted as PHAH. 0.250 g of Cu/γ-Al_2O_3 catalyst (5 wt% Cu loading) with a glass-covered magnetic stirring bar was reduced at 300℃ (temperature was ramped from 22 to 300℃ for 2 h) for 1 h under 34 bar (at 22℃) of H_2 gas in a Parr reactor. HAH feed solution was prepared by dissolving 1.12 g of HAH in an IPA/water cosolvent (IPA/water (mol) = 1/1, mixing 19.39 g of IPA solvent and 5.75 g of MQ water). The HAH feed solution was added by HPLC pump into the 50 mL Parr reactor, containing the reduced Cu/γ-Al_2O_3 catalyst under pressurized H_2 gas (~30 bar) to avoid catalyst oxidation by air contact. The reactor was purged twice with 50 bar of Ar gas and three times with 30 bar of H_2 gas. The reactor was pressurized to 35 bar of H_2 gas (at 22℃) and was heated to 120℃ in 35 min (final pressure increased to 45 bar at 120℃). The reactor was kept at 120℃ for 12 h with 450 rpm of stirring and cooled to room temperature by natural convection. The product solution was separated from the solid catalyst by syringe filter, and the cosolvent was evaporated by rotary evaporation (40℃, 30-100 mbar). The product was characterized by ^1H and ^{13}C NMR and was quantified by GC-FID. [21]

2.3 Synthesis of GA-MAL by imidation.

3.22 g (33 mmol) of maleic anhydride and 4.81 g (33 mmol) of L-glutamic acid were added into 31.5 g of acetic acid solvent in a 200 mL-scale round-bottom flask. The round flask was placed in an oil bath, set at 170℃, with reflux and reacted for 120 min under the stirring (600 rpm). The product solution was cooled to ~70℃ and the acetic acid solvent was evaporated by a rotary evaporator, set at 70℃, 110 rpm, 50-100 mbar, for 1 h. The concentrated product (orange colored sticky liquid) was placed in a vacuum oven (50℃, 500-600 mbar) for 22 h. The yield of GA-MAL was ~40 mol% and the concentrated product contained unreacted glutamic acid and maleic acid as a by-product. GA-MAL was purified by chromatography and characterized by ^{13}C qNMR (Chemical shift, δ: 172.53 (C1), 170.52 (C2), 170.29 (C1), 134.67 (C2), 50.62 (C1), 30.15 (C1), 23.58 (C1) ppm) and 2D HSQC NMR (Figure S13).

2.4 Synthesis of PHAH-GA-MAL by Diels-Alder reaction.

0.36 g (1.3 mmol) of PHAH and 0.58 g (2.6 mmol) of purified GA-MAL were added into 2.52 g of THF solvent to prepare a feed solution in a glass vial. The glass vial was capped to prevent the solvent from evaporation, and Diels-Alder reaction was carried out at room temperature (21-23℃) for 4 days. The conversion of GA-MAL reached ~100 mol% (Figure S4) by HPLC analysis. THF solvent was evaporated by rotary evaporation (40℃, 30-100 mbar), and PHAH-GA-MAL was characterized by ^{13}C qNMR (Chemical shift, δ: 209.02-208.56 (C1), 174.93 (C4), 174.86 (C2), 170.00 (C2), 137.54-137.24 (C2), 136.65-136.36 (C2), 92.40-92.31 (C2), 90.98-90.92 (C2), 60.14-60.10 (C2), 51.62-51.32 (C4), 48.01-47.88 (C2), 37.65 (C2), 30.47-30.44 (C2), 26.41 (C2), 23.48-23.45 (C2) ppm) and 2D HSQC NMR (Figure S14).

2.5 Synthesis of GA-MAL-H by hydrogenation.

0.13 g (0.55 mmol) of purified GA-MAL was added into 9.78 g of THF solvent to prepare a feed solution. 0.03 g of Ru/C (5 wt% Ru loading) and 9.86 g of the feed solution were added into a 50 mL-scale Parr reactor. The reactor was purged twice with 45 bar of Ar gas and three times with 30 bar of H_2 gas to remove air in the reactor. The reactor was pressurized to 40 bar of H_2 gas (at 22℃) and was heated to 30℃ in 20 min (final pressure increased to 42 bar at 30℃). The reactor was kept at 30℃ for 900 min with 450 rpm of stirring. The product solution was separated from the solid catalyst by syringe filter, and the cosolvent was evaporated by rotary evaporation (40℃, 30-100 mbar). The yield of GA-MAL-H was ~100 mol% and GA-MAL-H was characterized by ^{13}C qNMR (Chemical shift, δ: 177.07 (C2), 173.71 (C1), 169.89 (C1), 50.97 (C1), 30.04 (C1), 27.80 (C2), 22.87 (C1) ppm) and 2D HSQC NMR (Figure S15).

2.6 Synthesis of PHAH-GA-MAL-H by hydrogenation.

0.33 g (0.45 mmol) of the PHAH-GA-MAL was added into 8.00 g of THF solvent to prepare a feed solution. 0.06 g of Ru/C (5wt% Ru

loading) and 8.29 g of the feed solution were added into a 50 mL-scale Parr reactor. The reactor was purged twice with 45 bar of Ar gas and three times with 30 bar of H_2 gas to remove air in the reactor. The reactor was pressurized to 40 bar of H_2 gas (at 22℃) and was heated to 30℃ in 20 min (final pressure increased to 42 bar at 30℃). The reactor was kept at 30℃ for 900 min with 450 rpm of stirring. The product solution was separated from the solid catalyst by a syringe filter, and the cosolvent was evaporated by rotary evaporation (40℃, 30-100 mbar). The yield of PHAH-GA-MAL-H was ~100 mol% and PHAH-GA-MAL-H was characterized by ^{13}C qNMR (Chemical shift, δ: 209.06-208.87 (C1), 175.88 (C4), 175.76 (C2), 170.33 (C2), 89.16-88.84 (C2), 88.42-88.10 (C2), 61.43-61.34 (C2), 55.54-54.96 (C2), 51.84-51.73 (C2), 51.56-51.54 (C2), 37.35-37.25 (C2), 30.98-30.76 (C4), 30.73-29.89 (C4), 23.36 (C2) ppm) and 2D HSQC NMR (Figure S16). We note that impurities (e.g., maleic acid) sometimes deactivated the Ru/C catalyst during the first cycle of hydrogenation and showed no conversion of PHAH-GA-MAL. In such cases, the deactivated Ru/C was replaced and a second hydrogenation was repeated to achieve the full conversion of PHAH-GA-MAL.

2.7 Chromatography separation for the purification of GA-MAL.

The purification of GA-MAL was performed via column chromatography on a Biotage Isolera One unit with the aid of 120 g of a C_{18} Biotage Sfär reverse phase column. The separations were performed on 3 g portions of crude material utilizing a water/acetonitrile mobile phase. The mobile phase was swept from 0% to 5% acetonitrile for 7 column volumes, followed by an isocratic region at 5% acetonitrile for 3 column volumes. The column was washed with 100% water and 100% acetonitrile between each run.

2.8 Preparation of chemical-coating on silica and SBA-15 by pyrolysis.

0.473 g of sucrose was dissolved in MQ water (3.433 g, 6.974 g and 11.45 g of MQ water was used to wet silica, SBA-15 with 4 nm pores, and SBA-15 with 6 nm pores, respectively) to prepare sucrose solutions. Similarly, 0.462 g of acetamide was dissolved in 3.46 g of MQ water to prepare acetamide solution. The sucrose or acetamide solutions were added to 1.799 g of silica or SBA-15 with different pore sizes for wetness incipient impregnation. MQ water was evaporated in a fume hood by stirring the silica slurry for 17-21 h. 1.5 g of the chemical-containing silica was pyrolyzed at 200, 300, and 400℃ for 2 h under Ar gas flow (100 mL/min) to prepare C-coating (11 wt% of carbon) or N-doping (11 wt% of carbon with 6 wt% of nitrogen) of silica supports.

2.9 Immobilization of PHAH-GA-MAL-H (16 wt% catalyst loading) on various supports.

0.031 g (0.042 mmol) of PHAH-GA-MAL-H was added to 0.163 g of the engineered support in a glass vial. 0.24-0.35 g of THF solvent was added to the glass vial to dissolve PHAH-GA-MAL-H and wet the support. The catalyst slurry was sonicated and vortexed for a few minutes. THF solvent was evaporated by rotary evaporation (40℃, 350-400 mbar) for 70-130 min.

2.10 Reaction kinetics analysis for lactose hydrolysis.

0.66 g (1.85 mmol) of D-lactose monohydrate was added to 4.10 g of MQ water and heated at 100℃ to dissolve the lactose in water. 4.71 g of the lactose feed solution was added to 0.19 g of immobilized catalyst (or controlled amount of non-immobilized catalysts, such as sulfuric acid, glutamic acid, acetic acid, alanine, tyrosine, taurine, GA-MAL-H, and PHAH-GA-MAL-H) in a glass vial. The glass vial was capped to prevent the solvent from evaporation, and the hydrolysis reaction was carried out at 100℃ in an oil bath (120 and 90℃ were used to measure activation energies in Figure 3) with 600-800 rpm stirring. The glass vial reactor was centrifuged at 2500 rpm for 20 min to separate the immobilized catalyst before sampling. 0.1 mL of liquid sample solution was collected at each day (every 18-26 h) for 5 days and diluted in 0.4 mL of MQ water for the reaction kinetics analysis, and the diluted sample was filtered by syringe filter (20 μm pore) and analyzed by HPLC. The following equations (Equation1-4) were used as a kinetic model, and the rate constants for lactose hydrolysis (k_{app}) and glucose degradation ($k_{d,app}$) were measured by fitting the experimental kinetic data to the kinetic model by MATLAB with 95% confidential intervals.

$$\frac{d[Lactose]}{dt} = -k_{app}[Lactose] \quad \text{.....Eq.1}$$

$$\frac{d[Galactose]}{dt} = k_{app}[Lactose] \quad \text{.....Eq.2}$$

$$\frac{d[Glucose]}{dt} = k_{app}[Lactose] - k_{d,app}[Degraded\ Glucose] \quad \text{.....Eq.3}$$

$$\frac{d[Degraded\ Glucose]}{dt} = k_{d,app}[Degraded\ Glucose] \quad \text{.....Eq.4}$$

$$([Degraded\ Glucose] = [Galactose] - [Glucose])$$

k_{app} is the apparent rate constant for lactose hydrolysis, and $k_{d,app}$ is the apparent rate constant for glucose degradation, with 95% confidential intervals.

Each hydrolysis cycle was performed for 5 days (~110-122 h). After each hydrolysis cycle, the liquid solution was separated from the precipitated catalyst (by centrifuge at 2500 rpm, for 20 min). Then, a refreshed lactose feed solution was prepared by adding 0.66 g of D-lactose monohydrate into 4.10 g of MQ water and heating it at 100℃ to dissolve the lactose in water. 4.71 g of the refreshed feed solution was added to the wet catalyst for the next cycle of the hydrolysis for catalyst stability analysis. Catalyst stability analysis was performed by repeating the hydrolysis cycle for 3-4 times.

2.11 Lactose hydrolysis in the presence of $Ca(OAc)_2$.

The controlled amounts of $Ca(OAc)_2$ were added to a mixture of 0.974 g (2.70 mmol) of D-lactose monohydrate, 0.080 g (0.54 mmol) of L-glutamic acid, and 6.000 g (6.01 mL) of MQ water (where 0.000g, 0.0057 g, 0.0172 g, and 0.0251 g of calcium acetate hydrate were added to prepare 0, 5, 16, and 24 mM concentrations of $Ca(OAc)_2$ in the feed solution, respectively). The glass vial was capped to prevent the solvent from evaporation, and reaction was carried out at 100℃ in an oil bath with 800 rpm stirring. 0.1 mL of liquid sample solution was collected each day (every 18-26 h) for 5 days and diluted in 0.4 mL of MQ water for the reaction kinetics analysis. The diluted sample was analyzed by HPLC. Experimentally measured rates at different concentrations of $Ca(OAc)_2$ were analyzed by the kinetic model (Eq.1-4).

2.12 Extraction of the used PHAH-GA-MAL-H from the immobilized organocatalyst.

43 wt% loading of PHAH-GA-MAL-H on Si-C_4 support was prepared by the following method. 0.123 g (0.042 mmol) of PHAH-GA-MAL-H was added to 0.163 g of the engineered support in a glass vial. 0.24

g of THF solvent was added to the glass vial to dissolve PHAH-GA-MAL-H and wet the support. The catalyst slurry was sonicated and vortexed for a few minutes. THF solvent was evaporated by rotary evaporation (40℃, 350-400 mbar) for 70 min. The immobilized organocatalyst was used for 5th cycle of lactose hydrolysis over 400 h. The wet and used catalysts were separated from the hydrolyzed solution. 7 g of ethyl acetate (EtOAc) was added to the used catalyst and mixed with the used catalyst for 10 min for extraction of PHAH-GA-MAL-H. EtOAc layer was isolated and dried by rotary evaporation (40℃, 110-30 mbar) for 45 min. The extracted and dried PHAH-GA-MAL -H was dissolved in DMSO-d_6 for 2D HSQC NMR analysis (Figure S12).

2.13 HPLC analysis for the hydrolyzed lactose solution.

The chemical concentrations of hydrolyzed lactose solutions were quantified by high performance liquid chromatography (HPLC) analysis. The hydrolyzed solutions with immobilized catalysts were centrifuged (2500 rpm, 20 min) to separate the immobilized catalyst in the aqueous phase solution. 0.1 mL of the aqueous solution was diluted in 0.4 mL of Milli-Q water (5 times dilution by volume) to analyze the concentrations of lactose, glucose, galactose, and HMF as one of by-products by glucose degradation. The concentrations of lactose, glucose, galactose, glutamic acid, acetic acid, and GA-MAL-H in aqueous solution were measured by a Water 2695 separation module equipped with an Aminex HPX-87H (Bio-Rad) column and RI detector, while the HMF concentrations were measured with a Waters 2998 PDA detector, set at 320 nm. The temperature of the HPLC column was maintained at 50℃, and the flow rate of the mobile phase (pH 2 water, acidified by sulfuric acid) was 0.6 mL/min.

2.14 ^{13}C quantitative NMR analysis for characterization of organocatalysts.

^{13}C quantitative nuclear magnetic resonance (qNMR), and 2D HSQC NMR spectra were obtained using a Brucker Avance-500 spectrometer and analyzed by MNova software. Tetramethylsilane (TMS) (δ: 0 ppm) or deuterated solvents (DMSO-d_6) were used as a reference for chemical shifts. Experimental parameters for ^{13}C qNMR are as followings: Relaxation delay (D1) = 20 sec, Acquisition time (AQ) = 1 sec, Number of scans (NS) = 64, Number of dummy scans (DS) = 2, Spectral width (SW) = 284 ppm, Middle of spectrum (O1P) = 110 ppm, Size of fid (1TD) = 71424.

3. Results and discussion

3.1 Effect of different amino acids on lactose hydrolysis.

Site-directed amino acid substitutions, such as glutamic acid and tyrosine, in enzymes play a role in acid/base active sites for lactose hydrolysis. [33,34]. The catalytic activity for lactose hydrolysis was investigated by reaction kinetics analysis at 100℃ in the presence of various amino acids and terminated before complete conversion of lactose. As a result, the final conversion of lactose and the yield of glucose and galactose were <77 mol%, and the carbon balance (or material balance) was conserved (>95 mol%) during the hydrolysis. The concentration of amino acids was held constant (82-84 mM) to measure the catalytic activity (Figure 1). The apparent rate constants for lactose hydrolysis and glucose degradation were measured by the kinetic model (Eq.1-4). Glutamic acid showed the highest activity for lactose hydrolysis (k_{app}=0.0060 ± 0.0004 h^{-1}) among the amino acids, including taurine (k_{app}=0.0011 ± 0.0002 h^{-1}), tyrosine (k_{app}=0.0004 ± 0.0001 h^{-1}), and alanine (k_{app}=0.0005 ± 0.0001 h^{-1}). Consequently, the glutamic acid was appended onto the organocatalysts as an active functionality for the design of the organocatalysts due to its highest hydrolysis activity among the tested amino acids (Scheme 1a).

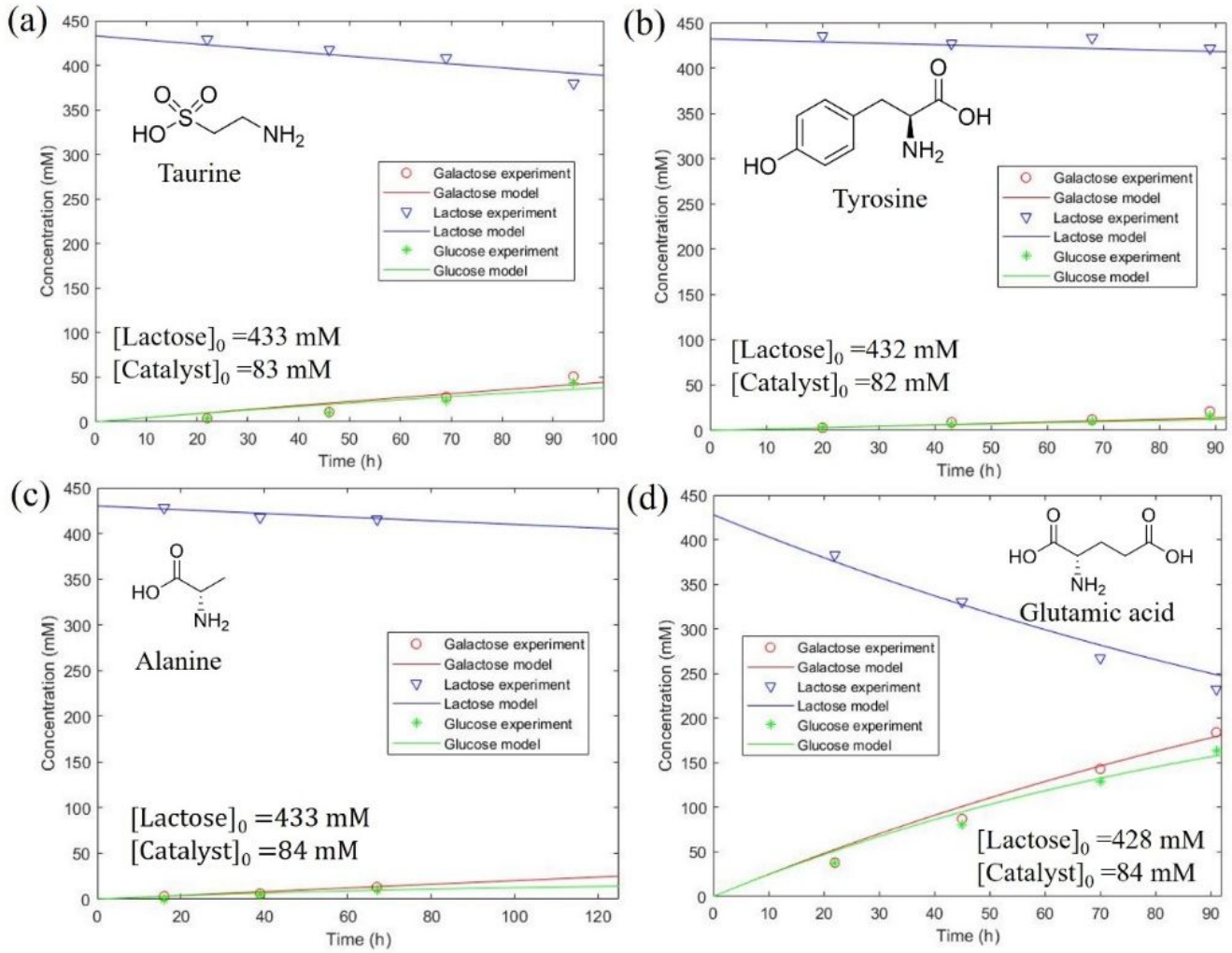

Figure 1. Reaction kinetics analysis for lactose hydrolysis (at 100℃) in presence of different amino acids, (a) taurine (k_{app}=0.0011 ± 0.0002 h^{-1}, $k_{d,app}$=0.0030 ± 0.0056 h^{-1}), (b) tyrosine (k_{app}=0.0004 ± 0.0001 h^{-1}, $k_{d,app}$=0.0005 ± 0.0116 h^{-1}), (c) alanine (k_{app}=0.0005 ± 0.0001 h^{-1}, $k_{d,app}$=0.0102 ± 0.0106 h^{-1}), and (d) glutamic acid (k_{app}=0.0060 ± 0.0004 h^{-1}, $k_{d,app}$=0.0027 ± 0.0018 h^{-1}). k_{app} and $k_{d,app}$ represent the apparent rate constants for lactose hydrolysis and glucose degradation, respectively and the values are evaluated within 95% confidential intervals.

3.2 Addition of $Ca(OAc)_2$ for the investigation of catalytic active site.

Lactose hydrolysis can occur on various active sites, such as free proton (H^+) and non-dissociated carboxylic acids, and each active site can possess different catalytic activity. For example, non-dissociated acetic acid (AA) showed lower catalytic activity than free proton (H^+) for lactose hydrolysis (Figure S1). The rate constant for H^+ (k_{H^+}) was determined to be 0.95 $M^{-1}\cdot h^{-1}$ by an independent experiment that used sulfuric acid as acid catalyst (Figure S1.a). The rate constant for the non-dissociated acetic acid (k_{AA}) was experimentally determined to be 0.0051 $M^{-1}\cdot h^{-1}$ by the following equation, $k_{app,\ AA} = k_{H^+}\cdot[H^+] + k_{AA}\cdot[AA]$, where [AA] and [$H^+$] were calculated by extrapolating the pK_a value from acetic acid dissociation ($pK_{a,AA}$=4.87 at 100℃). [35] The value of $k_{app,AA}$ ($k_{app,AA}$=0.0015 h^{-1}) was measured by the reaction kinetics analysis that used acetic acid as acid catalyst (Figure S1.b).

In Figure S2, the addition of $Ca(OAc)_2$ reduces the concentration of H^+ ([H^+]) by shifting thermodynamic equilibrium of acid dissociation. The reaction rates for the glutamic acid-catalyzed hydrolysis were affected by the concentration of $Ca(OAc)_2$ since the compositions of the active functionalities, such as H^+, acetic acid, and glutamic acid, depend on [$Ca(OAc)_2$] (Figure 2). Therefore, the different amounts of $Ca(OAc)_2$ were added to the lactose hydrolysis system to vary the concentrations of potential active sites in glutamic acid (i.e., G_1H, G_2H) at constant reaction temperature (100℃). Assumptions for the active site is required to determine the rate constant of the active site in glutamic acid, because glutamic acid has two carboxylic acids (i.e., G_1H, G_2H). For instance, when G_1H (side-chain carboxylic acid) is assumed as a single active site, the rate constant for G_1H (k_{G_1H}) was determined to be 1.0644 $M^{-1}\cdot h^{-1}$ by the following expression, $k_{app} = k_{H^+}\cdot[H^+] + k_{G_1H}\cdot[G_1H]$, where [$H^+$] and [$G_1H$] were calculated by solving the coupled equilibrium equations for glutamic acid dissociation (Figure S2) with the extrapolated pK_a values ($pK_{a,G1H}$ = 2.24, $pK_{a,G2H}$ = 4.55, $pK_{a,GNH}$ = 9.12 at 100℃ [36]). The value of k_{app} was measured by the reaction kinetics analysis in Figure 2a.

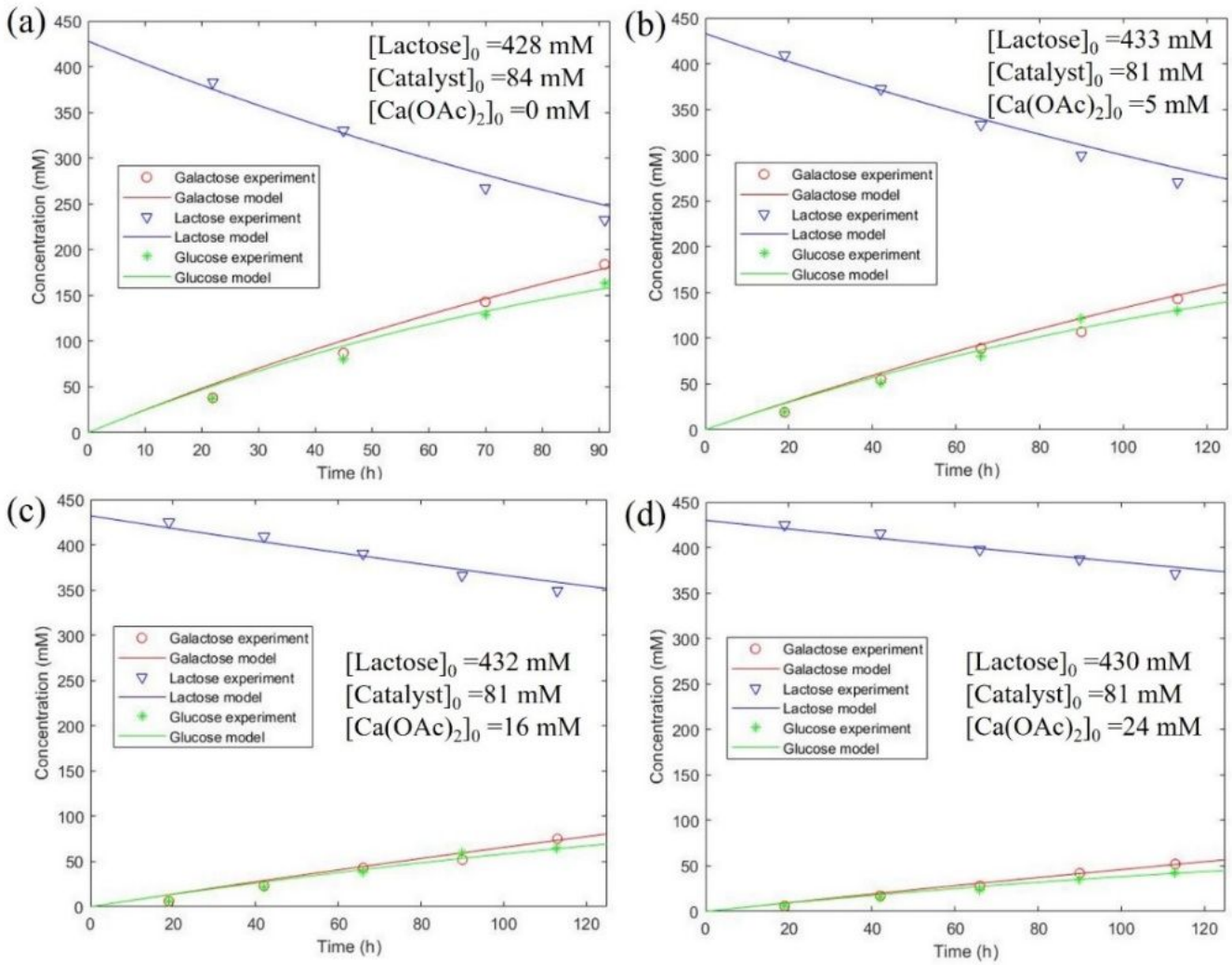

Figure 2. Reaction kinetics analysis for lactose hydrolysis (at 100°C) in the presence of different amounts of $Ca(OAc)_2$; where (a) $[Ca(OAc)_2]$= 0 mM, Rate=0.0026 M·h^{-1}, k_{app}=0.0060 ± 0.0004 h^{-1}, $k_{d,app}$=0.0027 ± 0.0018 h^{-1}, (b) $[Ca(OAc)_2]$= 5 mM, Rate=0.0016 M·h^{-1}, k_{app}=0.0037 ± 0.0002 h^{-1}, $k_{d,app}$=0.0020 ± 0.0013 h^{-1}), (c) $[Ca(OAc)_2]$= 16 mM, Rate=0.0007 M·h^{-1}, k_{app}=0.0016 ± 0.0001 h^{-1}, $k_{d,app}$=0.0023 ± 0.0018 h^{-1}), and (d) $[Ca(OAc)_2]$= 24 mM, Rate=0.0005 M·h^{-1}, k_{app}=0.0011 ± 0.0001 h^{-1}, $k_{d,app}$=0.0037 ± 0.0017 h^{-1}). k_{app} and $k_{d,app}$ represent the apparent rate constants for lactose hydrolysis and glucose degradation, respectively and the values are evaluated within 95% confidential intervals. (Glutamic acid served as catalyst).

Glutamic acid has three chemical functional groups: α-carboxylic acid (G_1H), side-chain carboxylic acid (G_2H), and amine (G_N), as shown in Figure 3. One or more functional groups in glutamic acid can become active sites for lactose hydrolysis. Accordingly, the active site for glutamic acid was specified by comparing the experimentally measured reaction rates with the theoretically predicted rates that assume the possible combination of each functional group to form the active site (Figure 3). Agreement between the theoretical rates and the experimental rates would then suggest that the assumed active site is the correct active site. The theoretically predicted rate (equation in Figure 3) was expressed by a linear combination of the rate constants and the concentrations of corresponding active sites. The kinetically determined values of k_{G_1H}, k_{AA}, and k_{H^+} were used to calculate the predicted rates in different concentration of $Ca(OAc)_2$. The concentrations of H^+, AA, and G_1H were varied by the concentration of $Ca(OAc)_2$ and determined by solving thermodynamic equilibrium of the acid dissociation (Figure S2). The good fit between the predicted and experimental rates indicates that G_1H is the precise active site from glutamic acid for lactose hydrolysis, as shown in Figure 3 (slope = 0.9091, R^2=0.9454). In contrast, when G_2H or the combination of G_1H and G_2H were assumed to be the active sites, predicted and experimental rates did not match well (Figure S3). As a result, the rate constants for the active site (G_1H) from the glutamic acid moieties in the presence of the organocatalysts were determined by the following equation, $k_{G_1H} = (k_{app} - k_{H^+} \cdot [H^+])/[G_1H]$, based on reaction kinetics (e.g., k_{app}, k_{H^+}) and thermodynamics (e.g., $[H^+]$, $[G_1H]$). The active site analysis enables differentiation of the contributions to the catalytic activity by H^+ (pH effect) and by the active site (G_1H) of organocatalysts. We emphasize that the k_{G_1H} value for each organocatalyst is the normalized rate constant by the number of active sites and then used to compare catalytic activities from the engineered organocatalysts in the following sections. Thereby, the experimental offsets in catalyst concentrations (73-84 mM in Figure 4) were adjusted by the

normalized rate constants (k_{G_1H}), and pH effect was also excluded to provide precise comparison of catalytic activities between organocatalysts. The active site analysis considers two glutamic acid moieties in the difunctional PHAH-GA-MAL-H to count the G_1H sites.

$$\text{Predicted rate} = (k_{H^+}\cdot[\mathrm{H^+}] + k_{AA}\cdot[\mathrm{AA}] + k_{G_1H}\cdot[\mathrm{G_1H}])\cdot[\mathrm{Lactose}]_0$$

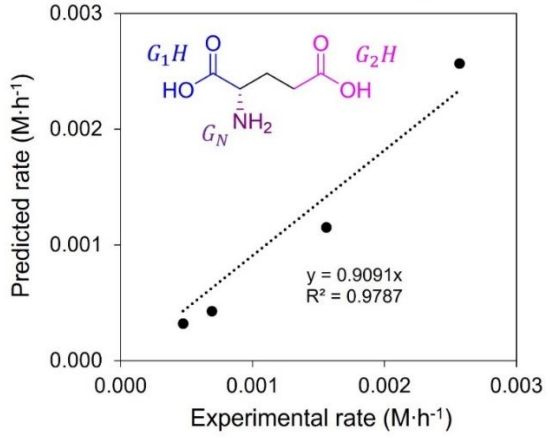

Figure 3. Active site analysis in glutamic acid by model fitting for the predicted and experimental rates for lactose hydrolysis in the presence of $Ca(OAc)_2$.

3.3 Effect of the engineered organocatalysts on lactose hydrolysis.

We engineered organocatalysts according to the strategy shown in Scheme 1a, and investigated the effect of the engineered organocatalysts on the catalytic activity for lactose hydrolysis. Glutamic acid was used to produce GA-MAL by imidation of glutamic acid (GA) and maleic anhydride (MAL). The C=C bond in the maleimide moiety of GA-MAL was hydrogenated to produce GA-MAL-H, because hydrogenation increases the stability against hydrothermal degradation of the organocatalyst and prevents side-reactions during lactose hydrolysis at 100°C. Figure 4 compares the reaction kinetics in the presence of the engineered organocatalysts. GA-MAL-H had 31.9% higher (from 1.06 to 1.40 $M^{-1}\cdot h^{-1}$) rate constant for the active site (k_{G_1H}) than k_{G_1H} for glutamic acid. Glucose degradation was observed as a side-reaction during lactose hydrolysis. The degree of glucose degradation was quantified by the ratio ($k_{d,app}/k_{app}$) of apparent rate constant for glucose degradation ($k_{d,app}$) and lactose hydrolysis (k_{app}), because this ratio represents relative rate of the degradation, based on the rate of lactose hydrolysis. In Figure 4a and b, the value of $k_{d,app}/k_{app}$ for GA-MAL-H ($k_{d,app}/k_{app}$=0.29) was 35.6% lower compared to $k_{d,app}/k_{app}$ for glutamic acid ($k_{d,app}/k_{app}$=0.45), and the result represents higher catalytic selectivity of GA-MAL-H than that of glutamic acid. The higher activity and selectivity of GA-MAL-H, compared to glutamic acid, may result from the imidation that suppresses basicity of the amine group.

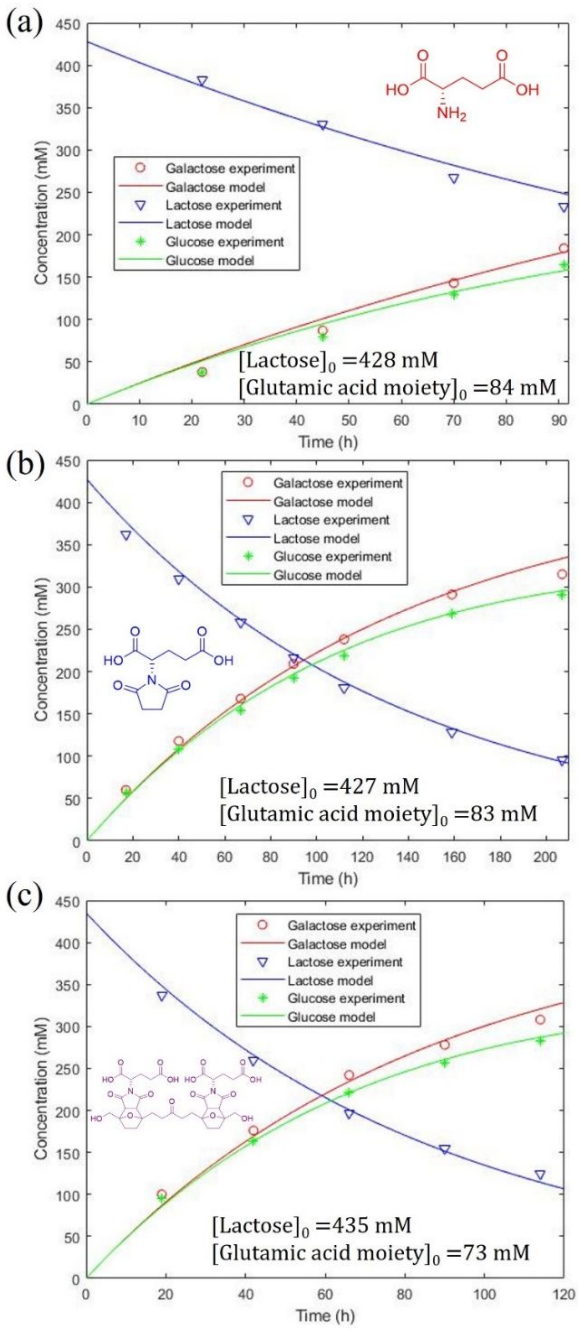

Figure 4. Reaction kinetics analysis for lactose hydrolysis over the non-immobilized organocatalysts, (a) glutamic acid (k_{app}=0.0060 ± 0.0004 h^{-1}, $k_{d,app}$=0.0027 ± 0.0018 h^{-1}), (b) GA-MAL-H (k_{app}=0.0077 ± 0.0002 h^{-1}, $k_{d,app}$=0.0022 ± 0.0008 h^{-1}), and (c) PHAH-GA-MAL-H (k_{app}=0.0117 ± 0.0004 h^{-1}, $k_{d,app}$=0.0016 ± 0.0005 h^{-1}). k_{app} and $k_{d,app}$ represent the apparent rate constants for lactose hydrolysis and glucose degradation, respectively and the values are evaluated within 95% confidential intervals.

GA-MAL was further upgraded to PHAH-GA-MAL by Diels-Alder reaction with a biomass-derived difuran (PHAH), and the conversion of GA-MAL (~100 mol%) is shown in Figure S4. No significant degradation of reactants was observed with NMR and HPLC analysis during the Diels-Alder reaction. PHAH-GA-MAL was also hydrogenated to saturate the C=C bonds and produce PHAH-GA-

MAL-H. The PHAH-GA-MAL-H complex has a difunctional glutamic acid moiety and higher hydrophobicity, compared to GA-MAL-H. The hydrophobicity of PHAH-GA-MAL-H (Limited solubility in water) and GA-MAL-H (solubility = 20.9 g/L in water) were quantified by measuring the water solubility of each molecule at room temperature. The PHAH-GA-MAL-H catalyst had a 74.2% higher rate constant for the active site (k_{G_1H}=2.45 $M^{-1}\cdot h^{-1}$) than GA-MAL-H (k_{G_1H} =1.40 $M^{-1}\cdot h^{-1}$). The value of $k_{d,app}/k_{app}$ for PHAH-GA-MAL-H ($k_{d,app}/k_{app}$=0.14) was half the value compared to $k_{d,app}/k_{app}$ for GA-MAL-H ($k_{d,app}/k_{app}$=0.29), as shown in Figure 4b and c. The higher activity and selectivity of PHAH-GA-MAL-H than GA-MAL-H implies that the difunctional G_1H site with higher hydrophobicity [37] may lead to the superior catalytic properties because two adjacent amino acid substitutions, such as Glu517 and Glu441, in the enzymatic active site contribute to the formation of a transition state of lactose for hydrolysis. [38] The distance between two active sites in the enzyme were calculated to be around 6.0 Å [38], and this value is consistent with the distance between two G_1H sites (7.35 Å, Figure S17) in PHAH-GA-MAL-H within 23%. This consistent distance (6-7 Å) between two active sites in the enzyme and the organocatalyst suggests that the controlled physical distance of two active sites gives rise to difunctionality that can assist the formation of transition states to catalyze hydrolysis. Thus, imidation and Diels-Alder reactions of glutamic acid derivatives not only improve the catalytic activity but also suppress the side-reaction during lactose hydrolysis. The molecular structures of the synthesized organocatalysts (GA-MAL, GA-MAL-H, PHAH-GA-MAL, PHAH-GA-MAL-H) were characterized by ^{13}C quantitative NMR (qNMR) and 2D HSQC NMR spectra (Figure S13-S26). The unassigned chemical shifts in ^{13}C NMR spectrum of PHAH-GA-MAL (Figure S14) resulted from PHAH [21] and GA-MAL (Figure S13), formed by retro Diels-Alder reaction during evaporation of THF solvent at 40℃. The splits and unassigned peaks in the spectrum of PHAH-GA-MAL-H (Figure S16) were exo-conformation of the Diels-Alder adducts. [17]

3.4 Immobilization of the organocatalyst on functionalized silica.

When the concentration of PHAH-GA-MAL-H increased from 37 to 70 mM, the value of k_{app} remained constant (Figure S5) because the organocatalyst reached the solubility limit (~37mM = 27.0 g/L in water at 100℃) of PHAH-GA-MAL-H in water (Figure S6). Immobilization of the organocatalyst on solid supporting materials can prevent aggregation of the organocatalyst by distributing the organocatalyst on the surface of the support. Figure 5a shows the schematic structure of the immobilized organocatalysts on support materials consisting of various functional groups on their surface. Catalytic reaction over the immobilized organocatalyst is analogous to the performance of enzymatic reactions. For analogy, an organocatalyst complex on a functionalized support with controlled surface properties can act in an analogous fashion as an active site in the channel of an enzyme. Reactants bind on the active site (G_1H sites) by the interaction between surface functionality on the support and the organocatalyst. Lower loading amounts of organocatalyst on the support enhanced the catalytic activity (Figure 5b). This result suggests that the lower catalyst loading prevents the catalyst aggregation or improves the interaction between the organocatalyst and support by providing a more uniform distribution of the organocatalyst on the support.

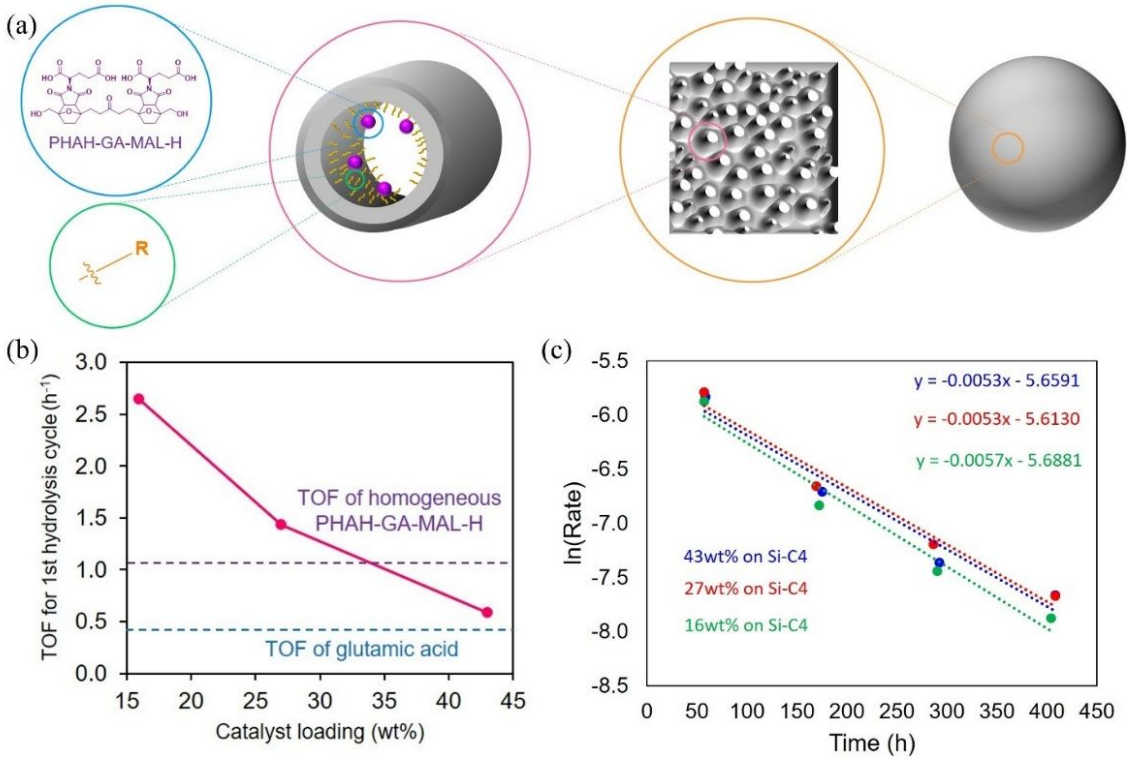

Figure 5. (a) Graphical structure of organocatalysts (R- represents surface functionality of the support); (b) Turnover frequency (TOF) for lactose hydrolysis as a function of the loading amounts of PHAH-GA-MAL-H on Si-C_4 support; (c) Catalyst stability (16wt% PHAH-GA-MAL-H was supported on Si-C_4) for lactose hydrolysis. (Slope represents rate constant for catalyst deactivation ($k_{deact.}$), y-intercept shows log-scale initial rate for lactose hydrolysis (ln($Rate_0$) and $Rate_0$ was used to calculate k_{G_1H} and TOF for the active site.)

Catalyst deactivation was observed upon the repeated reaction cycles of lactose hydrolysis, but the deactivation is independent of the catalyst loading amounts (Figure 5c). The main cause of catalyst deactivation is leaching of the organocatalyst into solution since PHAH-GA-MAL-H is soluble in water (27.0 g/L in water at 100℃). Also, there was hydrothermal degradation of the leached organocatalyst. Glutamic acid was produced during the lactose hydrolysis in the presence of GA-MAL-H and PHAH-GA-MAL-H (Figure 6b and c). The yield of glutamic acid by degradation remained constant after the immobilization on different functionalized silica supports, such as Si-C_4 and Si-diol (Figure 6d and e). Another reason for deactivation can be the accumulation of the organocatalysts on the supports as the color of the used immobilized catalyst turned darker during repeated catalytic reaction cycles (Figure S7). [32]

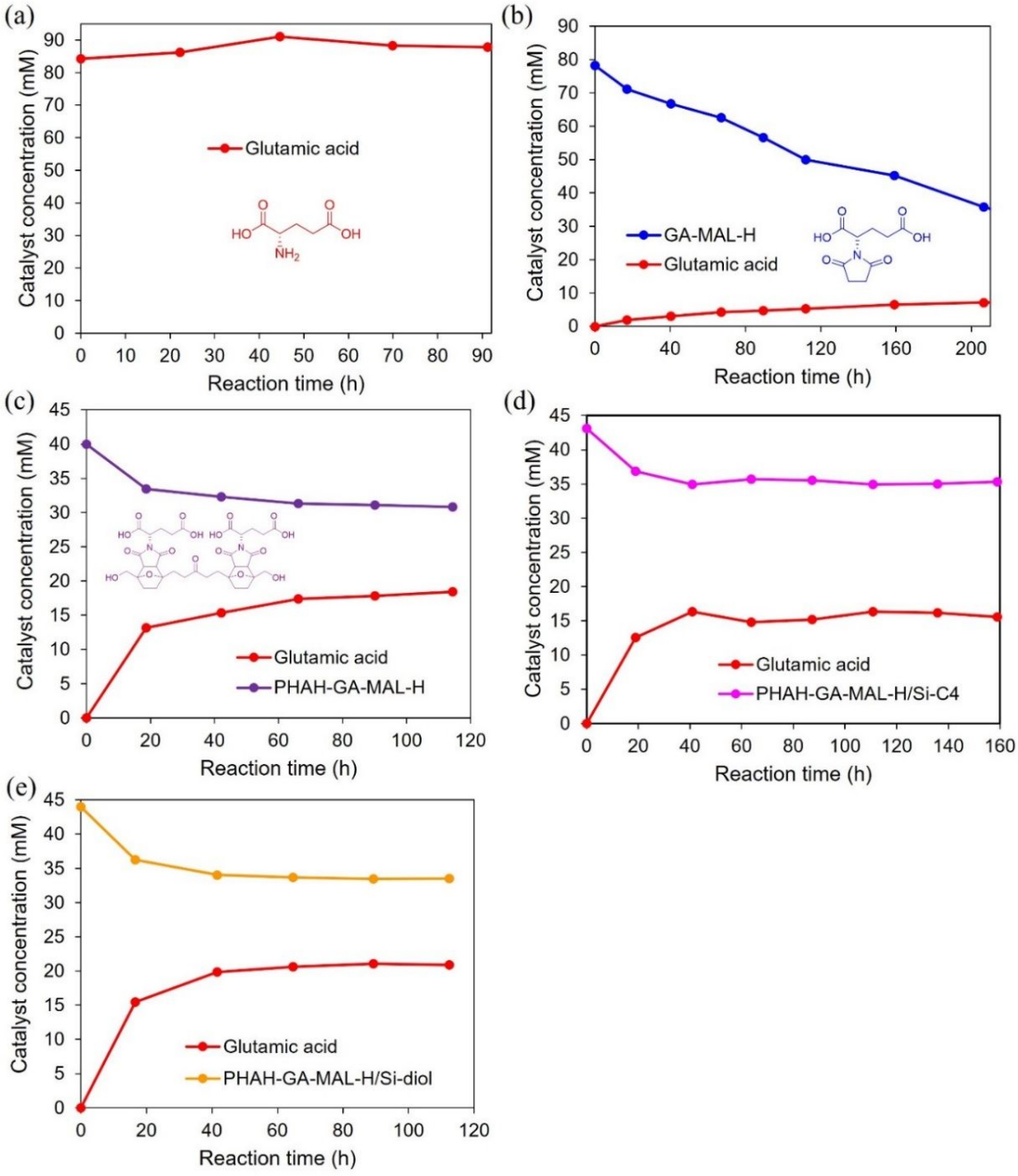

Figure 6. Hydrothermal degradation during lactose hydrolysis at 100℃ of (a) glutamic acid, (b) GA-MAL-H, (c) non-immobilized PHAH-GA-MAL-H, (d) PHAH-GA-MAL-H (43wt% loading) on Si-C_4, and (e) PHAH-GA-MAL-H (43wt% loading) on Si-diol. (Degradation of PHAH-GA-MAL-H produced glutamic acids and the yield of glutamic acid was analyzed by HPLC; [PHAH-GA-MAL-H] = $[\text{PHAH-GA-MAL-H}]_0$ – [Glutamic acid]/2).

3.5 Effect of reaction temperature on catalytic activity and stability.

The reaction temperature was varied from 90 to 120℃ to measure the activation energies for lactose hydrolysis and hydrothermal catalyst deactivation, and results are shown in Figure 7. Decreasing the temperature to lower than 90℃ showed no measurable rates of lactose hydrolysis. Moreover, increasing temperature did not improve the relative rate of lactose hydrolysis versus catalyst

deactivation because the activation energy for lactose hydrolysis (107 kJ/mol) and catalyst deactivation (116 kJ/mol) are similar (Figure 7d). The used PHAH-GA-MAL-H, immobilized on Si-C_4 support (43wt% loading) was recollected by extraction in ethyl acetate (EtOAc) solvent after the 5th cycle of lactose hydrolysis over 520 h of reaction. The extracted PHAH-GA-MAL-H from the used catalyst was characterized by the 2D HSQC NMR spectrum (Figure S12), and the weight of the extracted organocatalyst was measured to calculate the yield of catalyst recollection. The recollection yield of the used PHAH-GA-MAL-H from the support was calculated to be ≤5.0 wt%, indicating that the organocatalyst degraded and accumulated on the supports during lactose hydrolysis.

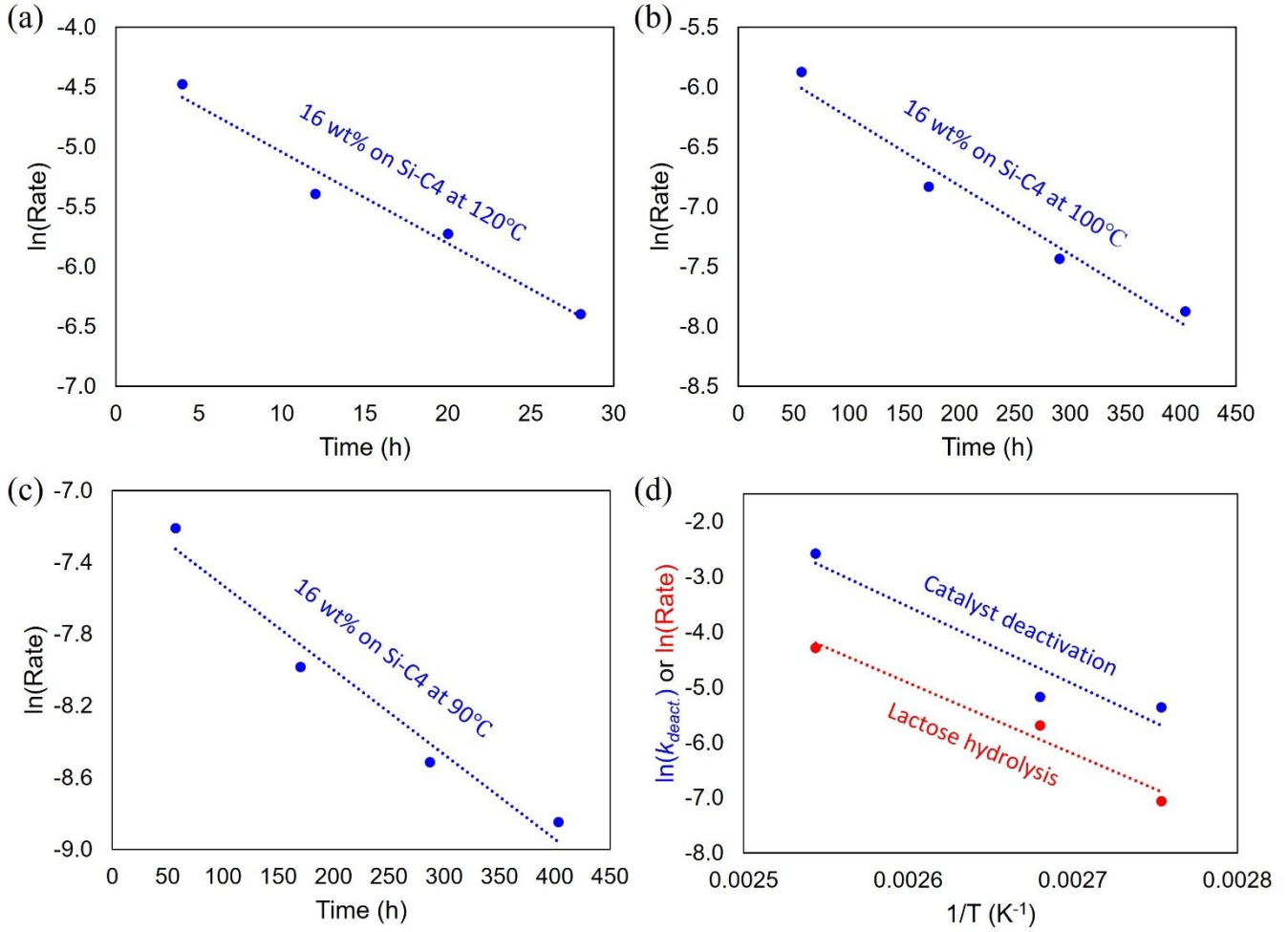

Figure 7. Catalyst activity (turnover frequency, TOF) over reaction time at different reaction temperatures (a) 120°C (slop= -0.0762), (b) 100°C (slop= -0.0057), (c) 90°C (slop= -0.0047) and (d) Van't hoff plot for catalyst deactivation (blue, slop= -13978) and lactose hydrolysis (red, slop= -12838); Activation energy for catalyst deactivation and lactose hydrolysis is 116 and 107 kJ/mol, respectively.

3.6 Effect of supporting materials on the catalytic properties.

Various commercial supporting materials were prepared without further characterization and used to immobilize the organocatalyst. The effect of the supports on the catalytic activity (as quantified by the rate constant for the active site, k_{G_1H}) is summarized in Figure 8. The activity of sulfuric acid was measured to represent the catalytic activity of synthetic catalysts since it is the most commonly used catalyst for hydrolysis processes. PHAH-GA-MAL-H (k_{G_1H}=2.45 ± 0.08 $M^{-1}h^{-1}$) showed 2.6 times higher activity than sulfuric acid (k_{H+} =0.95 ± 0.04 $M^{-1}h^{-1}$) and provided 2.3 times higher k_{G_1H} than glutamic acid (k_{G_1H}=1.06 ± 0.03 $M^{-1}h^{-1}$) which has the highest activity among the non-immobilized chemical catalysts (homogeneous reaction system at 100°C). 16 wt% loading of catalyst immobilization on the methyl-functionalized silica (Si-C_1) support (k_{G_1H}=5.50 ± 0.15 $M^{-1}h^{-1}$) showed 2.2 times higher TOF than the homogenous PHAH-GA-MAL-H (k_{G_1H} =2.45 ± 0.08 $M^{-1}h^{-1}$).

Support materials with different functional groups can affect the interaction between lactose and the G_1H active site. The balance between hydrophobicity and hydrophilicity of the support can alter the catalytic activity, because appropriate hydrophobic [37] and hydrophilic interactions [31] are necessary to mimic enzyme structures, possessing combinations of hydrogen bonds and hydrophobic channels from aromatic residues that comprise the enzymatic active site. [30] Accordingly, various functionalized silicas with different length of carbon chains were used to investigate the effect of different surface properties of the silica supports. The silica support functionalized with -C_1 (k_{G_1H}=5.50 ± 0.15 $M^{-1}h^{-1}$) and -C_4 groups (k_{G_1H} =5.32 ± 0.25 $M^{-1}h^{-1}$) had ~30% higher activity than -diol (k_{G_1H}=4.18 ± 0.19 $M^{-1}h^{-1}$) and -C_{18} functionalized silica (k_{G_1H}=4.18 ± 0.12 $M^{-1}h^{-1}$). Consequently, -C_1 and -C_4 functionalities on silicas contributed to the higher catalytic activity for lactose hydrolysis than -C_{18} and -diol groups. Pyrolysis of diverse chemicals, such as sucrose and

acetamide, over silica can provide carbon (C) coating or nitrogen-atom (N) doping on the surface of the support. [39] Moreover, pyrolysis temperature affected the surface functionality of the chemical-coating supports and tailored the catalytic activity by modifying the amounts of -OH groups, which can catalyze glucan hydrolysis by the formation of hydrogen bond between the Brønsted acidic -OH sites and the glycosidic oxygen. [31] A pyrolysis temperature at 200°C resulted in higher k_{G_1H} (k_{G_1H}=4.80 ± 0.15 $M^{-1}h^{-1}$) than the C-coating support treated by higher pyrolysis temperature (k_{G_1H}= 3.83 ± 0.14 and 3.74 ± 0.24 $M^{-1}h^{-1}$ for 300 and 400°C pyrolysis). The controlled porous structure of silica (SBA-15) with different pore sizes (4 and 6 nm) did not show a difference in catalytic activity (k_{G_1H}= 3.74 ± 0.24, 3.57 ± 0.13 and 3.66 ± 0.05 $M^{-1}h^{-1}$ for random pore silica, SBA-15 with 4 nm pore, and 6 nm pore, respectively). N-doping on the support displayed 61.6% lower k_{G_1H} (k_{G_1H}=2.87 ± 0.08 and 2.95 ± 0.13 $M^{-1}h^{-1}$) than C-coated supports (k_{G_1H}= 3.57 ± 0.13 and 4.80 ± 0.15 $M^{-1}h^{-1}$) suggesting that N-doping sites may serve as basic sites. An acidic support (TiO_2) [40] had a value of k_{G_1H} (k_{G_1H}=5.41 ± 0.19 $M^{-1}h^{-1}$) as high as Si-C_1 support likely due to the acidic properties of the TiO_2 support where 32.3% of the apparent rate constants for hydrolysis (k_{app}) over PHAH-GA-MAL-H supported on TiO_2 resulted from the bare TiO_2 support (Figure S8.a and d). Carbon-based supports (i.e., silicon-carbide) had lower k_{G_1H} (k_{G_1H}=2.60 ± 0.16 $M^{-1}h^{-1}$) than the functionalized silica supports (k_{G_1H}= 4.18 ± 0.12 and 5.50 ± 0.15 $M^{-1}h^{-1}$). These results suggest that the surface properties, altered by different preparation methods for supports, can significantly affect the catalytic activity.

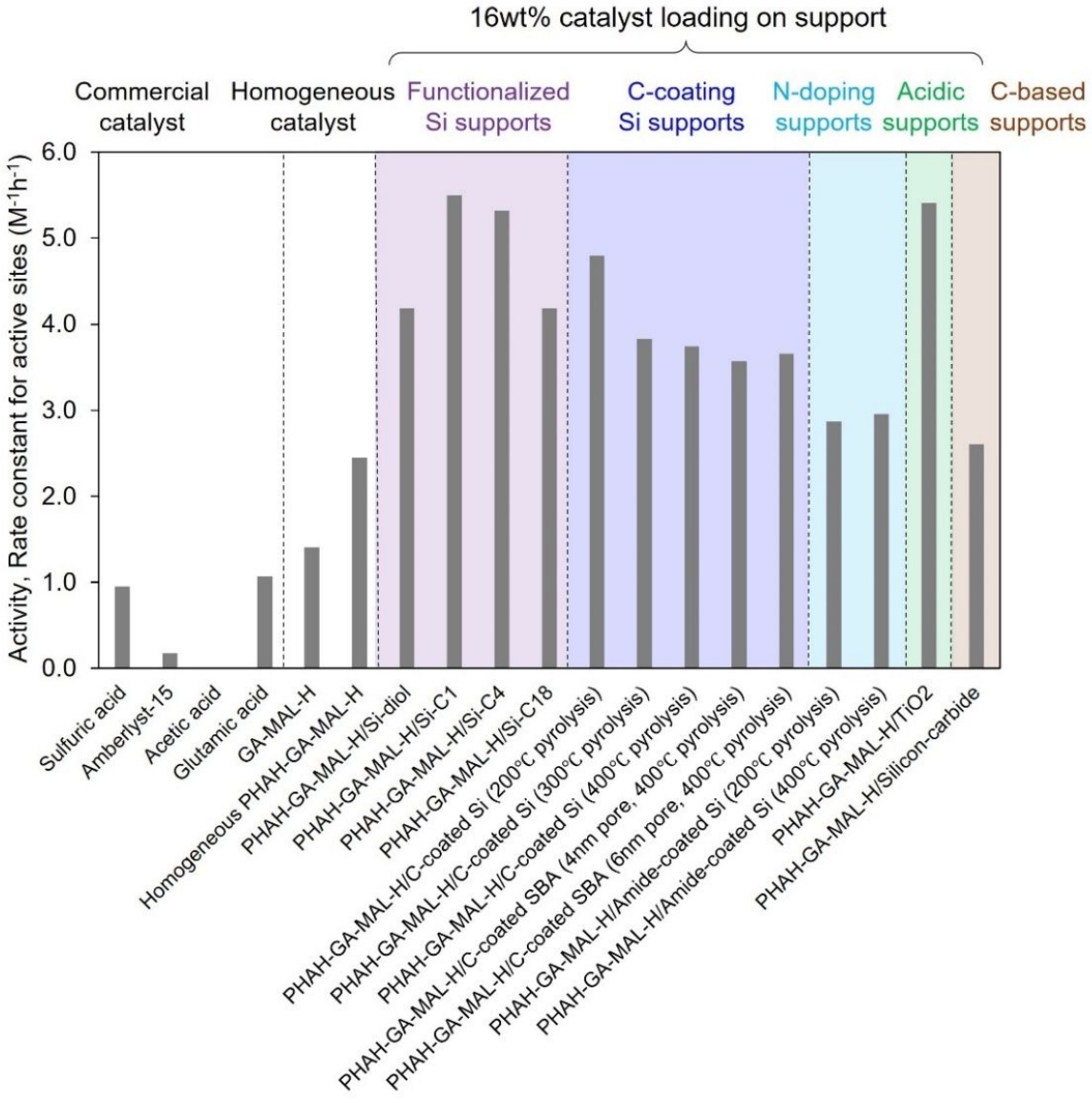

Figure 8. Effect of various supports on catalytic activity (where rate constants were measured from the 1st cycle of hydrolysis).

Figure S9 summarizes the catalytic stability, selectivity, and total turnover numbers for the supported organocatalysts. The silicon-carbide support was the only support with no catalyst deactivation (Figure S10), but this catalyst showed lower catalytic activity. All other supports represented similar degree of catalyst deactivation ($k_{deact.}$ = 0.0031-0.0057 h^{-1}). Catalyst selectivity (Figure S9.b) was assessed by the ratio ($k_{app}/k_{d,app}$) between the rate of the target reaction (lactose hydrolysis, k_{app}) and the rate of the undesired reaction (glucose degradation, $k_{d,app}$), measured by kinetic analysis of the first cycle of lactose hydrolysis. Si-C_4 and C-coated Si (treated by

200℃ pyrolysis) supports showed the highest selectivity ($k_{app}/k_{d,app}$ ~4.00). Additionally, the carbon balance remained >95 mol% throughout the entire cycles of lactose hydrolysis (~400 h) in the presence of the immobilized organocatalysts, which leads to a higher catalytic selectivity. The <5 mol% loss of carbons resulted from the thermal degradation of glucose (Scheme 1b). Total turnover numbers ($TON = \frac{\Delta N_{lactose}}{N_{site,0}}$) of the deactivating catalysts over 400 h on stream were calculated by Equation 6 (rearranging Equation 5, with t = 400 h). $k_{deact.}$ and initial rates for lactose hydrolysis were determined from the slope and the y-intercept (=ln($Rate_0$)) of catalyst stability plots (Figure S11), and values of $Rate_0$ were used to calculate $k_{G_1H}$and *TOF* (turnover frequency) for the active sites. Total turnover numbers ($TON = \frac{\Delta N_{lactose}}{N_{site,0}}$) of the non-deactivating catalysts were calculated by Equation 7.

$$\Delta N_{lactose} = \int_0^t Rate\ dt = TOF \cdot N_{site,0} \int_0^t e^{-k_{deact.}t} dt \quad \text{.....Eq.5}$$

$$TON = \frac{\Delta N_{lactose}}{N_{site,0}} = TOF \cdot \int_0^t e^{-k_{deact.}t} dt = TOF \cdot \left(\frac{1 - e^{-k_{deact.}t}}{k_{deact.}}\right) \text{..Eq.6}$$

$$TON = \text{TOF from averaged rate (h -1)} \cdot \text{Operation time (h)} \quad \text{.....Eq.7}$$

In Figure S9.c, total turnover numbers for the immobilized catalysts on amide-coated silicas (TON=310-330) and silicon-carbide supports (TON=295) were lower than functionalized silica (TON=350-515) and C-coated silica (TON=360-425). It appears that supports with Si-C_1 and C-coated silica at 300℃ pyrolysis yielded the highest total turnover numbers. Bare supports without the immobilized catalyst had negligible catalytic activities (k_{app}=0.0005-0.0008 h^{-1}) for lactose hydrolysis, except the acidic support (TiO_2) (Figure S8.a). The turnover numbers for PHAH-GA-MAL-H on TiO_2 (TON=575) included the effect of acidic support. We note that the turnover frequencies (h^{-1}) of the immobilized organocatalysts are an order of magnitude lower than those for enzymatic hydrolysis using engineered enzymes. [23]

Conclusions

We have illustrated new approaches to design organocatalysts, and we have demonstrated the tunable catalytic properties of these materials for lactose hydrolysis as a model reaction. Glutamic acid was incorporated as the N group in maleimide (GA-MAL), and Diels-Alder reaction was used to combine the GA-MAL on a difuran molecule (PHAH) to synthesize a difunctional organocatalyst (PHAH-GA-MAL). The organocatalyst was then hydrogenated (PHAH-GA-MAL-H) to increase the thermal stability, and this moiety was used for lactose hydrolysis. The hydrophobicity and difunctionality of PHAH-GA-MAL-H produced 2.3 times higher catalytic activity compared to glutamic acid. The organocatalyst was immobilized various solid supports to mimic the active site channels in the protein matrix of enzymes. 16 wt% loading of the organocatalyst on silica-based supports improved the catalytic activity by 5.2 times compared to glutamic acid, and the surface functionalities of the supporting materials also affected the catalytic properties. These chemical-based catalysts are advantageous for efficient of downstream processes because they do not require biological broths for operation. Further advantages of these supported organocatalysts are that they can tailor the appropriate catalytic properties for various reactions by engineering the nature of the active sites in the structures of organocatalysts and by fabricating appropriate surface properties of the supports to be analogous to enzyme catalysts. For example, imidation of maleic anhydride with diamines or tertiary amines can produce organocatalysts for base-catalyzed reactions, such as aldol-condensation. In addition, future work for developing new biomimetic catalysts can be the synthesis of N-substituted maleimides with various amino acids (e.g., aspartic acid, glutamine, histidine) and the immobilization of the organocatalysts with different ratios of amino acids to mimic the active sites in enzymes for hydrolysis of polysaccharides. Importantly, larger complexes containing 3 furan groups can be formed by sequential aldol condensation reactions of diformylfurans with ketones, thereby providing new strategies for the synthesis of "catalytic triads" (such as combinations including glutamic acid, aspartic acid, histidine, and tyrosine) that have been reported in the enzyme catalysis literature. [27] More active catalysts formed in this manner would then allow for operation at lower temperatures, closer to those temperatures used for enzymatic reactions.

Author Contributions

Conceptualization: HC, GWH, JAD; Methodology: HC, AGS; Investigation: HC; Visualization: HC, GWH, JAD; Funding acquisition: GWH, JAD; Project administration: JAD; Supervision: GWH, JAD; Writing – original draft: HC, AGS, GWH, JAD; Writing – review & editing: HC, GWH, JAD.

Conflicts of interest

Hochan Chang, George W. Huber, and James A. Dumesic have submitted a provisional patent application related to this work filed by the Wisconsin Alumni Research Foundation. Alexios G. Stamoulis declares that he has no competing interests.

Acknowledgements

We thank the NMR facilities funded by: Thermo Q ExactiveTM Plus by NIH 1S10 OD020022-1; Bruker Quazar APEX2 and Bruker Avance-500 by a generous gift from Paul J. and Margaret M. Bender; Bruker Avance-600 by NIH S10 OK012245; Bruker Avance-400 by NSF CHE-414 1048642 and the University of Wisconsin-Madison.

Notes and references

1 D. M. Alonso, S. G. Wettstein and J. A. Dumesic, *Chem. Soc. Rev.*, 2012, **41**, 8075–8098.
2 J. Baruah, B. K. Nath, R. Sharma, S. Kumar, R. C. Deka, D. C. Baruah and E. Kalita, *Front. Energy Res.*, 2018, **6**, 141.
3 H. Chang, I. Bajaj, A. H. Motagamwala, A. Somasundaram, G. W. Huber, C. T. Maravelias and J. A. Dumesic, *Green Chem.*, 2021, **23**, 3277–3288.
4 A. H. Motagamwala, K. Huang, C. T. Maravelias and J. A. Dumesic, *Energy Environ. Sci.*, 2019, **12**, 2212–2222.
5 T. Thananatthanachon and T. B. Rauchfuss, *Angew. Chemie*, 2010, **122**, 6766–6768.

6 A. H. Motagamwala, W. Won, C. Sener, D. M. Alonso, C. T. Maravelias and J. A. Dumesic, *Sci. Adv.*, , DOI:10.1126/SCIADV.AAP9722/SUPPL_FILE/AAP9722_SM.PDF.
7 S. E. Davis, L. R. Houk, E. C. Tamargo, A. K. Datye and R. J. Davis, *Catal. Today*, 2011, **160**, 55–60.
8 E. De Jong, M. A. Dam, L. Sipos and G. J. M. Gruter, *ACS Symp. Ser.*, 2012, **1105**, 1–13.
9 C. L. Williams, C.-C. Chang, P. Do, N. Nikbin, S. Caratzoulas, D. G. Vlachos, R. F. Lobo, W. Fan and P. J. Dauenhauer, *ACS Catal.*, 2012, **2**, 935–939.
10 R. Lee, J. R. Vanderveen, P. Champagne and P. G. Jessop, *Green Chem.*, 2016, **18**, 5121.
11 R. M. West, Z. Y. Liu, M. Peter, C. A. Gärtner and J. A. Dumesic, *J. Mol. Catal. A Chem.*, 2008, **296**, 18–27.
12 S. Li, F. Chen, N. Li, W. Wang, X. Sheng, A. Wang, Y. Cong, X. Wang and T. Zhang, *ChemSusChem*, 2017, **10**, 711–719.
13 Y.-T. Cheng and G. W. Huber, *Green Chem.*, 2012, **14**, 3114–3125.
14 J. J. Pacheco and M. E. Davis, *Proc. Natl. Acad. Sci.*, 2014, **111**, 8363–8367.
15 M. Gregoritza and F. P. Brandl, *Eur. J. Pharm. Biopharm.*, 2015, **97**, 438–453.
16 S. Kotha and S. Banerjee, *RSC Adv.*, 2013, **3**, 7642–7666.
17 H. Chang, G. W. Huber and J. A. Dumesic, *ChemSusChem*, 2020, **13**, 5213–5219.
18 S. Higson, F. Subrizi, T. D. Sheppard and H. C. Hailes, *Green Chem.*, 2016, **18**, 1858.
19 B. Kim, J. Lee, H. Y. Bae, S. U. Son and C. Song, *Macromol. Rapid Commun.*, 2022, 2200711.
20 H. Chang, A. H. Motagamwala, G. W. Huber and J. A. Dumesic, *Green Chem.*, 2019, **21**, 5532–5540.
21 E. B. Gilcher, H. Chang, M. Rebarchik, G. W. Huber and J. A. Dumesic, *ACS Catal.*, 2022, 10186–10198.
22 H. Chang, E. B. Gilcher, G. W. Huber and J. A. Dumesic, *Green Chem.*, 2021, **23**, 4355–4364.
23 N. Hassan, B. Geiger, R. Gandini, B. K. C. Patel, R. Kittl, D. Haltrich, T. H. Nguyen, C. Divne and T. C. Tan, *Appl. Microbiol. Biotechnol.*, 2016, **100**, 3533–3543.
24 T. Vasiljevic and P. Jelen, *Innov. Food Sci. Emerg. Technol.*, 2001, **2**, 75–85.
25 P. J. T. Dekker, D. Koenders and M. J. Bruins, *Nutrients*, 2019, **11**, 551.
26 T. Hasunuma, F. Okazaki, N. Okai, K. Y. Hara, J. Ishii and A. Kondo, *Bioresour. Technol.*, 2013, **135**, 513–522.
27 M. D. Nothling, Z. Xiao, N. S. Hill, M. T. Blyth, A. Bhaskaran, M. A. Sani, A. Espinosa-Gomez, K. Ngov, J. White, T. Buscher, F. Separovic, M. L. O'Mara, M. L. Coote and L. A. Connal, *Sci. Adv.*, 2020, **6**, eaaz0404.
28 R. C. Rodrigues, C. Ortiz, Á. Berenguer-Murcia, R. Torres and R. Fernández-Lafuente, *Chem. Soc. Rev.*, 2013, **42**, 6290–6307.
29 A. Jungbauer and N. Walch, *Curr. Opin. Chem. Eng.*, 2015, **10**, 1–7.
30 B. C. Knott, M. F. Crowley, M. E. Himmel, J. Ståhlberg and G. T. Beckham, *J. Am. Chem. Soc.*, 2014, **136**, 8810–8819.
31 O. M. Gazit and A. Katz, *J. Am. Chem. Soc.*, 2013, **135**, 4395–4402.
32 J. Y. Chen and N. A. Brunelli, *Energy and Fuels*, 2021, **35**, 14885–14893.
33 R. R. Mahoney, *Food Chem.*, 1998, **63**, 147–154.
34 C. G. Cupples, J. H. Miller and R. E. Huber, *J. Biol. Chem.*, 1990, **265**, 5512–5518.
35 H. S. Harned and R. W. Ehlers, *J. Am. Chem. Soc.*, 1933, **52**, 652–656.
36 H. Nagai, K. Kuwabara and G. Carta, *J. Chem. Eng. Data*, 2008, **53**, 619–627.
37 R. Breslow, *J. Phys. Org. Chem.*, 2006, **19**, 813–822.
38 M. Rutkiewicz, A. Bujacz, M. Wanarska, A. Wierzbicka-Wos and H. Cieslinski, *Int. J. Mol. Sci.*, 2019, **20**, 4301.
39 H. N. Pham, A. E. Anderson, R. L. Johnson, T. J. Schwartz, B. J. O'neill, P. Duan, K. Schmidt-Rohr, J. A. Dumesic and A. K. Datye, *ACS Catal.*, 2015, **5**, 4546–4555.
40 B. Krishnakumar and M. Swaminathan, *J. Mol. Catal. A Chem.*, 2011, **334**, 98–102.